Dopant homogeneity and transport properties of impurity-doped oxide nanowires

Annop Klamchuen,[1] Takeshi Yanagida,[1,2,a)] Masaki Kanai,[1] Kazuki Nagashima,[1] Keisuke Oka,[1] Shu Seki,[3] Masaru Suzuki,[4] Yoshiki Hidaka,[4] Shoichi Kai,[4] and Tomoji Kawai[1,b)]

[1]*Institute of Scientific and Industrial Research, Osaka University, 8-1 Mihogaoka, Ibaraki, Osaka 567-0047, Japan*
[2]*PRESTO, Japan Science and Technology Agency, 4-1-8 Honcho, Kawaguchi, Saitama 332-0012, Japan*
[3]*Division of Applied Chemistry, Graduate School of Engineering, Osaka University, 2-1 Yamadaoka, Suita, Osaka 565-0871, Japan*
[4]*Department of Applied Quantum Physics and Nuclear Engineering, Faculty of Engineering, Kyushu University, 744 Motooka, Nishi-ku, Fukuoka 819-0395, Japan*

(Received 14 December 2010; accepted 10 January 2011; published online 3 February 2011)

Controlling and understanding an impurity doping on semiconductor oxide nanowires grown by the vapor-liquid-solid (VLS) method remains an important challenge. Homogeneous dopant distribution within oxide nanowires has been assumed without the direct evaluations to interpret the transport properties. Here we report the direct measurements of dopant distributions for Ta-doped SnO_2 nanowires. We find that differences in dopant incorporations between VLS and vapor-solid growth processes give rise to a heavily doped shell surrounding an underdoped core. Thus, understanding the dopant incorporation pathways is essential to designing and controlling impurity doping on VLS grown oxide nanowires. © *2011 American Institute of Physics*. [doi:10.1063/1.3549703]

Recent advanced semiconductor technology requires the precise control of an impurity doping on semiconductors to develop functional devices. Such controllability is also strongly required for vapor-liquid-solid (VLS) grown semiconductor nanowires toward functional nanowire device applications.[1–5] Especially, the dopant distribution within nanowires has been a critical issue recently.[6–9] For example, Perea *et al.* have performed the atom probe tomography to visualize the three-dimensional dopant distributions in Ge nanowires.[6] Koren *et al.* investigated the active dopant distribution of phosphorus within Si nanowires by combining the field effect transistor and the sequential surface etching process.[7] Previous reports consistently demonstrated the importance of the dopant distribution mostly for conventional semiconductor nanowires including Si, Ge, and compounds. Metal oxide nanowires are emerging potential candidates to add new functionalities such as transparent conductivity, ferroelectricity, and nonvolatile memory, which are hardly attainable in conventional semiconductors.[10,11] Studies have been reported as to the effects of impurity doping on the electrical and magnetic properties of various VLS grown oxide nanowires.[12,13] Especially VLS grown SnO_2 nanowires with impurity doping have been intensively studied due to their transparent conductivity;[13–15] for example, Ta-doped SnO_2 nanowires.[13] In these impurity-doped oxide nanowires, the uniform dopant distribution within oxide nanowires has been assumed without the direct evaluations to interpret the electrical properties.[13–15] Here we report the direct measurements of dopant distributions for Ta-doped SnO_2 nanowires. We find that differences in dopant incorporations between VLS and vapor-solid (VS) growth processes give rise to an inhomogeneity of dopant distribution, highlighting the importance of controlling the dopant incorporation pathways during VLS growth of oxide nanowires.

Ta-doped SnO_2 nanowires were grown on Al_2O_3 (110) single crystal substrates by Au catalyst-assisted pulsed laser deposition technique (ArF excimer laser, $\lambda = 193$ nm).[16] The background pressure of the chamber was 7.0×10^{-6} Pa. Sn metal and Ta_2O_5 mixed powders were milled and compressed to fabricate targets with varying Ta dopant concentrations. Ta dopant concentration (Ta at. %) is hereafter defined as Ta/(Ta+Sn). Oxygen and argon mixed gas was introduced into the chamber with the ambient total pressure of 10 Pa. The flux ratio of oxygen and argon was 1:1000.[17] Prior to the laser ablation, the Au (0.7 nm)-coated Al_2O_3 substrate was preheated at the growth temperature of 750 °C for 20 min.[18] After the nanowire growth, the samples were cooled down to room temperature (RT) within 30 min. The microstructure of the nanowires was characterized by field emission scanning electron microscopy (FESEM, Hitachi S-4300) at an accelerating voltage of 30 kV. High-resolution transmission electron microscopy (HRTEM, JEOL JEM-3000F) with energy dispersive spectroscopy (EDS) was used to evaluate the diameter, crystallinity, and macroscopic composition of nanowires. HRTEM measurement was performed at an accelerating voltage of 300 kV. Scanning transmission electron microscopy (STEM, JEOL JEM-ARM200F, and FEI Tecnai Osiris™) at an acceleration voltage of 200 kV was employed to characterize the microscopic composition of nanowires. The probe size was ~0.19 nm in JEM-ARM200F and ~0.25 nm in Tecnai Osiris™, respectively. The transport properties were measured by a microwave conductivity measurement (MCM) at RT. To estimate quantitatively the resistivity of nanowires from MCM data, the nanowire density and the nanowire length were measured from data of FESEM images. The microwave frequency and power were set at ~9.1 GHz and 3 mW, respectively. The conductivity ($\Delta\sigma$) of the sample is related to the reflected

a)Electronic mail: yanagi32@sanken.osaka-u.ac.jp.
b)Electronic mail: kawai@sanken.osaka-u.ac.jp.

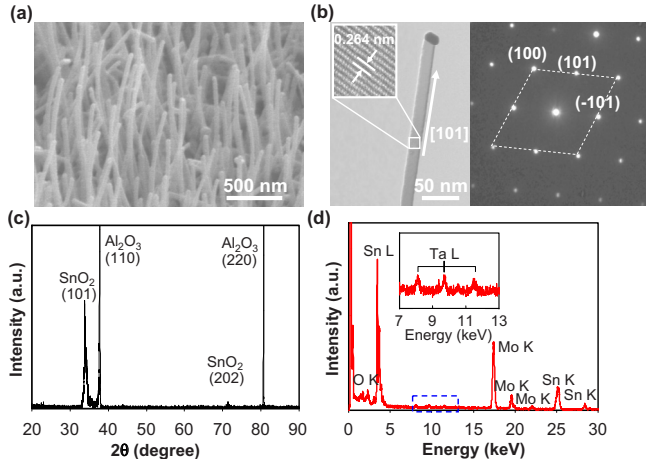

FIG. 1. (Color online) (a) FESEM image, (b) HRTEM image with SAED pattern, (c) XRD data, and (d) EDS data of Ta (1 at. %)-doped SnO_2 nanowires. The inset of EDS data shows the magnified data around Ta L shell peaks.

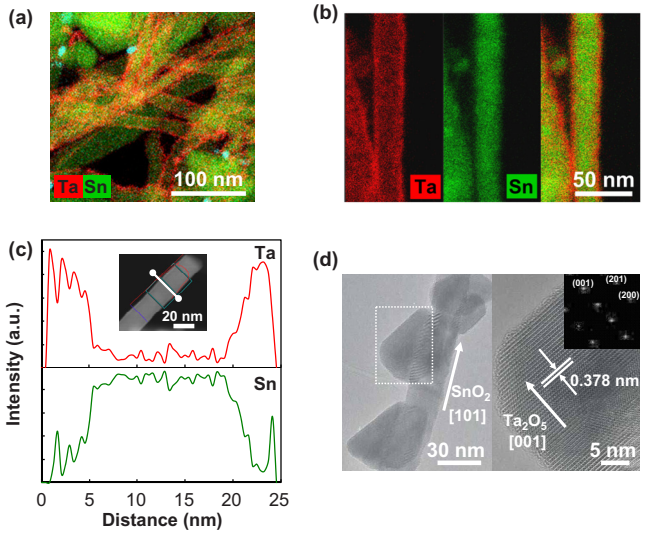

FIG. 3. (Color online) (a) STEM/EDS mapping images of Ta 1 at. % doped SnO_2 nanowires at low magnification. (b) STEM/EDS mapping images of Ta and Sn of Ta 1 at. % doped SnO_2 nanowires. (c) Line profile data of Sn and Ta for Ta 5 at. % doped SnO_2 nanowires. The inset shows STEM images. (d) HRTEM image and FFT pattern of Ta (20 at. %)-doped SnO_2 nanowires.

microwave power at the resonance frequency ($\Delta P_r/P_r$) via the formula of $\Delta\sigma=(1/A)(\Delta P_r/P_r)$, where A is a sensitivity factor. The other details of the set of apparatus were described elsewhere.[19,20] Previously, we have revealed the applicability of MCM for VLS grown oxide nanowires by comparing with dc contact transport measurements.[21]

Figure 1(a) shows the typical scanning electron microscopy (SEM) image of Ta-doped SnO_2 nanowires grown onto a single crystal Al_2O_3 (110) substrate. The Ta concentration in the target was 1 at. %. SnO_2 nanowires were grown almost perpendicular to the substrate. The occurrence of nanowire growth was confirmed for the range of Ta concentrations in the target at least up to 5 at. %. Figure 1(b) shows the HRTEM image of the fabricated SnO_2 nanowires with the selected area electron diffraction (SAED) pattern. The single crystalline nature and the [101] oriented growth of nanowires can be seen. X-ray diffraction (XRD) data also supports the [101] oriented nanowire growth, as shown in Fig. 1(c). Figure 1(d) shows the EDS measurement data, which were performed for an approximately several ten nm^2 area. It can be seen that Ta *L* shell peaks are observed, demonstrating macroscopically the presence of Ta within nanowires. Figure 2 shows the relationship between the nominal Ta concentration in the target and the incorporated macroscopic Ta concentration measured by EDS. The incorporated macroscopic Ta concentration was almost consistent with the nominal Ta concentration within the accuracy of EDS.[21] Figure 2 also shows the correlation between the nominal Ta concentration and the RT resistivity of nanowires measured by MCM. The resistivity systematically decreased with the increasing nominal Ta concentration. Obviously, there is a reasonable correlation between the resistivity and the incorporated macroscopic Ta concentration. The above results consistently imply successful Ta doping into VLS grown SnO_2 nanowires as reported in previous works.[13] However, the model based on a homogeneous dopant distribution[21] estimates the dopant activation of 0.67% for the Ta (5 at. %)-doped SnO_2 nanowires, which is extremely low and clearly not realistic when comparing with the dopant activation (90%) for Ta-doped SnO_2 films.[22] Therefore, we question the homogeneity of dopants incorporated into oxide nanowires in the following discussion.

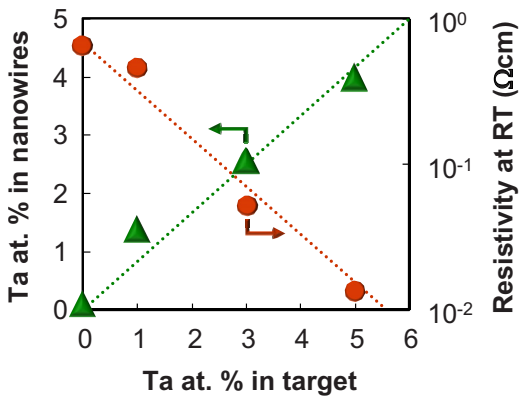

FIG. 2. (Color online) Ta concentration incorporated in nanowires and the resistivity with varying Ta concentration.

Figures 3(a) and 3(b) show the STEM/EDS mapping images of Ta (1 at. %)-doped SnO_2 nanowires. The distribution of Ta dopants is clearly inhomogeneous, with a heavily doped shell surrounding a core of much lower Ta concentration. The presence of the heavily doped shell layer was confirmed up to Ta 5 at. %. Figure 3(c) shows the concentration line profiles of Ta and Sn along the radial direction, which were measured for Ta (5 at. %)-doped SnO_2 nanowires. Quantitatively, the profiles must be interpreted as data projected for a cross-sectional area. Adapting the simple core/shell structure model,[23] we numerically analyzed the Ta concentration and the doping depth of the heavily doped area. The calculated doping depth and Ta concentration in the heavily doped shell are ~1 nm and >40 at. %, respectively. The remaining issue is what is responsible for the electrical conduction of Ta-doped SnO_2 nanowires, and where. First, we exclude the presence of a conductive outer shell layer because the estimated Ta concentration of >40 at. % seems to be beyond the limit of doping regime. Second, we consider the situation that the Ta-rich most outer shell is insulative as the Ta oxides and the inner region are

conductive. The model calculation[21] indicates that the inner region has 1.33×10^{-2} Ω cm of the resistivity. This means that only 0.05 at. % of Ta concentration for the inner region is required to explain the experimental resistivity data for Ta (5 at. %)-doped SnO_2.[22] The conductive inner region might be created via either Ta diffusion from the nanowire surface or Ta incorporation through catalysts. The formation of insulative Ta-oxides on the nanowire surface was confirmed more clearly in Ta (20 at. %)-doped SnO_2 nanowires, as shown in Fig. 3(d). The crystalline Ta_2O_5 on the nanowire surface was observed. Since Ta oxides including Ta_2O_5 are well-known insulators, the results seem to support the scenario based on a conductive inner region.

In principle, there are two major pathways for the dopant solidification process, which are the VLS process through metal catalysts and the VS process on the nanowire surface. Although the VLS pathway is desirable for a homogeneous dopant distribution, our results highlight that the major pathway for Ta solidification is an uncatalysed VS process. Another experimental evidence to support the VS pathway can be given by thin film VS experiments in the absence of metal catalysts. The VS experiments were performed under the same conditions as the VLS experiments. The Ta concentration of fabricated thin films (in the case of Ta 5 at. % nominal concentration) was over 95%, i.e., Ta-rich phases are easily formed via the VS growth process. Thus, all our experimental results consistently support the uncatalysed VS pathway for Ta solidification process. Next, we discuss what essentially determines the major pathway of dopants in VLS grown oxide nanowires. Within the classical framework of VLS, supplied atoms must be selectively incorporated into metal catalysts. Therefore, it is essential to prevent an uncatalysed VS surface growth to realize a well-defined VLS growth. This criterion must be applicable even for impurity dopants. In the case of Ta doping, the vapor pressure of Ta is rather low compared with that of Sn;[24] for example, the vapor pressures of Ta and Sn at 900 °C are $\sim10^{-16}$ and 10^{-4} mbar, respectively.[24] Thus, the VS surface growth of Ta compounds must easily occur under the present experimental conditions, which is consistent with our VS experiments. Previously we have clarified that the high vapor pressure of Sn allows us to fabricate untapered SnO_2 nanowires by preventing the VS growth of Sn oxides.[25] In this context, Ta seems to be not ideal to realize a homogeneous impurity doping in a VLS process with Sn oxides. To overcome this inhomogeneous issue, it would be essential to choose the dopant species whose vapor pressure is reasonably high and comparable to that of parent compounds. For SnO_2 nanowires, Indium might be a good candidate as dopant when considering the vapor pressure.[24,26]

In summary, we present the direct measurements of dopant distributions within Ta-doped SnO_2 nanowires. We find that differences in dopant incorporations between VLS and VS growths give rise to a heavily doped shell surrounding an underdoped core. We believe that understanding and controlling the dopant incorporation pathways by choosing appropriately the dopant species is essential to design impurity doping on VLS grown oxide nanowires. This seems to be a rather universal design rule for impurity doping on various VLS grown semiconductor oxide nanowires.

This study was in part supported by a Grant-in-Aid for Scientific Research on Innovative Areas (Grant No. 20111004) from the Ministry of Education, Culture Sports, Science, and Technology (MEXT) of Japan. T.K. was supported by the FIRST program.

[1]Y. Wu, Y. Cui, L. Huynh, C. J. Barrelet, D. C. Bell, and C. M. Lieber, Nano Lett. **4**, 433 (2004).
[2]W. Lu and C. M. Lieber, J. Phys. D **39**, R387 (2006).
[3]C. Yang, Z. Zhong, and C. M. Lieber, Science **310**, 1304 (2005).
[4]B. Tian, T. Cohen-Karni, Q. Qing, X. Duan, P. Xie, and C. M. Lieber, Science **329**, 830 (2010).
[5]P. C. Chen, G. Shen, H. Chen, Y. G. Ha, C. Wu, S. Sukcharoenchoke, Y. Fu, J. Liu, A. Facchetti, T. J. Marks, M. E. Thompson, and C. Zhou, ACS Nano **3**, 3383 (2009).
[6]D. E. Perea, E. R. Hemesath, E. J. Schwalbach, J. L. Lensch-Falk, P. W. Voorhees, and L. J. Lauhon, Nat. Nanotechnol. **4**, 315 (2009).
[7]E. Koren, N. Berkovitch, and Y. Rosenwaks, Nano Lett. **10**, 1163 (2010).
[8]R. A. Schlitz, D. E. Perea, J. L. Lensch-Falk, E. R. Hemesath, and L. J. Lauhon, Appl. Phys. Lett. **95**, 162101 (2009).
[9]D. E. Perea, E. Wijaya, J. L. Lensch-Falk, E. R. Hemesath, and L. J. Lauhon, J. Solid State Chem. **181**, 1642 (2008).
[10]K. Nagashima, T. Yanagida, K. Oka, M. Taniguchi, T. Kawai, J.-S. Kim, and B. H. Park, Nano Lett. **10**, 1359 (2010).
[11]J. R. Morber, Y. Ding, M. S. Haluska, Y. Li, J. P. Liu, Z. L. Wang, and R. L. Snyder, J. Phys. Chem. B **110**, 21672 (2006).
[12]S. Han, C. Li, Z. Liu, B. Lei, D. Zhang, W. Jin, X. Liu, T. Tang, and C. Zhou, Nano Lett. **4**, 1241 (2004).
[13]E. N. Dattoli, Q. Wan, W. Guo, Y. Chen, X. Pan, and W. Lu, Nano Lett. **7**, 2463 (2007).
[14]Q. Wan, E. N. Dattoli, and W. Lu, Appl. Phys. Lett. **90**, 222107 (2007).
[15]J. Huang, A. Lu, B. Zhao, and Q. Wan, Appl. Phys. Lett. **91**, 073102 (2007).
[16]K. Nagashima, T. Yanagida, H. Tanaka, and T. Kawai, J. Appl. Phys. **101**, 124304 (2007); A. Marcu, T. Yanagida, K. Nagashima, H. Tanaka, and T. Kawai, *ibid.* **102**, 016102 (2007); T. Yanagida, A. Marcu, H. Matsui, K. Nagashima, K. Oka, K. Yokota, M. Taniguchi, and T. Kawai, J. Phys. Chem. C **112**, 18923 (2008); A. Marcu, T. Yanagida, K. Nagashima, K. Oka, H. Tanaka, and T. Kawai, Appl. Phys. Lett. **92**, 173119 (2008); K. Nagashima, T. Yanagida, A. Klamchuen, M. Kanai, K. Oka, S. Seki, and T. Kawai, *ibid.* **96**, 073110 (2010).
[17]T. Yanagida, K. Nagashima, H. Tanaka, and T. Kawai, Appl. Phys. Lett. **91**, 061502 (2007).
[18]K. Nagashima, T. Yanagida, H. Tanaka, and T. Kawai, Appl. Phys. Lett. **90**, 233103 (2007); T. Yanagida, K. Nagashima, H. Tanaka, and T. Kawai, J. Appl. Phys. **104**, 016101 (2008).
[19]Y. Yamamoto, T. Fukushima, Y. Suna, N. Ishii, A. Saeki, S. Seki, S. Tagawa, M. Taniguchi, T. Kawai, and T. Aida, Science **314**, 1761 (2006).
[20]K. Nagashima, T. Yanagida, H. Tanaka, S. Seki, A. Saeki, S. Tagawa, and T. Kawai, J. Am. Chem. Soc. **130**, 5378 (2008); K. Oka, T. Yanagida, K. Nagashima, H. Tanaka, S. Seki, M. Ishimaru, A. Hirata, and T. Kawai, Appl. Phys. Lett. **95**, 133110 (2009).
[21]A. Klamchuen, T. Yanagida, K. Nagashima, S. Seki, K. Oka, M. Taniguchi, and T. Kawai, Appl. Phys. Lett. **95**, 053105 (2009).
[22]H. Toyosaki, M. Kawasaki, and Y. Tokura, Appl. Phys. Lett. **93**, 132109 (2008).
[23]S. K. Lim, M. J. Tambe, M. M. Brewster, and S. Gradečak, Nano Lett. **8**, 1386 (2008).
[24]H. R. Kerp, M. W. M. van Cleef, A. B. Wit, and R. E. I. Schropp, J. Vac. Sci. Technol. A **17**, 611 (1999).
[25]A. Klamchuen, T. Yanagida, M. Kanai, K. Nagashima, K. Oka, T. Kawai, M. Suzuki, Y. Hidaka, and S. Kai, Appl. Phys. Lett. **97**, 073114 (2010).
[26]Q. Wan, E. N. Dattoli, W. Y. Fung, W. Guo, Y. Chen, X. Pan, and W. Lu, Nano Lett. **6**, 2909 (2006).